ACS Catalysis

Research Article

pubs.acs.org/acscatalysis

DFT Prediction of Oxygen Reduction Reaction on Palladium−Copper Alloy Surfaces

Yao Sha, Ted H. Yu, Boris V. Merinov,* and William A. Goddard, III*

Materials and Process Simulation Center, California Institute of Technology, MC 139-74, Pasadena, California 91125, United States

ABSTRACT: The high cost of proton exchange membrane fuel cells (PEMFCs) comes largely from the use of platinum-containing electrocatalysts. Despite significant progress made the past decade on reducing the platinum catalyst loading in the PEMFC electrodes, further substantial cost reductions require the replacement of platinum with less expensive nonplatinum electrocatalytic materials. In this study, PdCu alloys have computationally been investigated as possible non-Pt catalysts for oxygen reduction reaction (ORR) in PEMFCs. We used density functional theory (DFT) calculations to determine the structural preference and ORR activity as a function of the composition and structure. Five PdCu alloy surface structures, B2, $L1_2$, $L1_0$, $L1_1$-nonlayered, and $L1_1$-layered, were considered, and the layered $L1_1$ surface structure was found to exhibit significantly improved ORR kinetics compared to that of pure Pd.

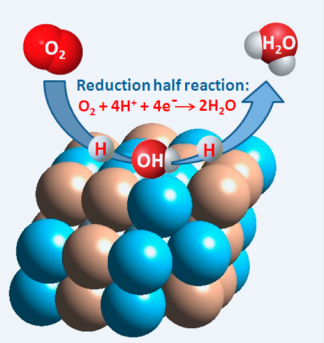

KEYWORDS: *DFT, ORR, PdCu alloys, surfaces, reaction mechanisms*

1. INTRODUCTION

The high cost of proton exchange membrane fuel cells (PEMFCs) is largely due to using platinum-containing electrocatalysts in this type of fuel cell. There is great interest in searching for advanced and cheaper cathode catalysts for a PEMFC that will maintain or even improve the performance of the ORR exhibited by Pt.[1−4] In the past decade, significant progress has been made in reducing the platinum metal loading in the PEMFC electrodes (see, for instance, ref 5). However, any further substantial cost reductions will require the replacement of platinum with a less expensive electrocatalytic material. A possible way to reach this goal is development, characterization, modeling, and fuel cell testing of nonplatinum metal-based alloys with the emphasis on achieving high ORR activity and material stability.

Catalytic metals with the highest stability in strongly acidic conditions are noble metals, such as rhodium, platinum, palladium, iridium, and gold.[6] Of these, platinum has the highest activity for the ORR with palladium being the second most active metal.[7] Nørskov et al. assumed that the reactivity of the transition metals correlates with the corresponding electronic structures (in particular, with the position of the d-band center) and forms a volcano-type plot.[8−11] From this model, it was predicted that only materials with the d-band center position, falling into a relatively narrow interval around the d-band center of Pt, may provide a high ORR catalytic activity. The electronic properties of the transition metals, including the d-band center position, can be modified by alloying them with metals that will shift the d-band center toward the desired position. Using density functional theory (DFT) calculations, Nørskov et al.[12] calculated the expected shift of the d-band center of an "impurity" metal on the surface of a bulk comprised of another metal. According to the d-band center hypothesis, PdCu alloys may have an improved ORR activity compared to pure Pd.[13] In our paper, we will discuss various crystal and surface structures of PdCu alloys and predict ORR rates for these systems.

2. COMPUTATIONAL METHODS

To study ORR, surfaces of PdCu catalyst systems are modeled as a slab infinite in two directions, *a* and *b*, and finite in the third direction *c*. We consider a 2 × 2 supercell-slab of the (111) surface (4 atoms per layer) composed of six layers (24 atoms). The top four layers, which represent the active surface, were allowed to relax, whereas the bottom two layers, representing the bulk, were fixed. The same model was applied in our previous calculations of pure Pt and Pt-based binary alloys.[14−18]

We used the SeqQuest code[19] with an optimized double-ζ plus polarization Gaussian type basis set contracted from calculations on the most stable unit cell of the pure elements. Small core angular-momentum-projected norm-conserving nonlocal effective core potentials[20−23] (pseudopotentials) were employed to replace the core electrons. Thus, the neutral Cu atom was described with 17 explicit electrons (six 3p, one 4s, and ten 3d in the ground state), whereas neutral Pd included 16 electrons of the 4p and 4d orbitals. In all calculations, we employed the kinetic and exchange-correlation DFT functional developed by Perdew, Burke, and Ernzerhof (PBE).[24]

The real space grid density was 5 points per Angstrom, while the reciprocal space grid was 5 × 5 × 0 for slab calculations. All calculations allowed the up-spin orbitals to be optimized independently of the down spin orbitals (spin-unrestricted periodical DFT).

For the solvated phase, we employed a continuum model[14] based on the Poisson−Boltzmann approximation.[25−28] All reaction pathways were determined using the nudged elastic band (NEB)[29,30] method, and solvent effects were included for each point along the path.

Received: July 1, 2013
Revised: January 24, 2014
Published: February 24, 2014

   dx.doi.org/10.1021/cs4009623 | *ACS Catal.* 2014, 4, 1189−1197

For the ordered bulk structures, we used fcc and bcc cubic unit cells with 4 and 2 atoms per cell, respectively, relaxing both the atoms and cell parameters. The reciprocal space grid was 12 × 12 × 12. For the solid solution (disordered) bulk structures, we randomly placed Pd and Cu atoms in a 2 × 2 × 1 fcc unit cell with 16 atoms. The atoms and volumes of the unit cells were allowed to relax. The reciprocal space grid was 6 × 6 × 12. Although we will further call these phases as fcc- and bcc-type, strictly speaking, they are not really fcc or bcc but rather have Pd and Cu atoms distributed over the fcc- or bcc-type lattice.

3. RESULTS AND DISCUSSION

3.1. Bulk Structures and Energetics. Figure 1 shows a phase diagram for the Pd−Cu binary system. The following three unique phases can be identified:

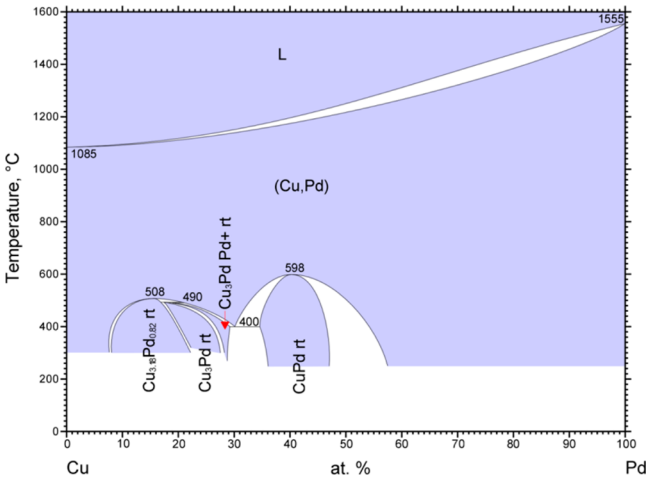

Figure 1. Phase diagram of the PdCu system.[31] Three unique phases can be identified: (1) bcc- type phase at around 45% atomic ratio, (2) fcc-type $PdCu_3$, and (3) fcc-type solid solution (Cu, Pd) phase.

(1) a distinct PdCu phase with the B2 (CsCl) bcc-type structure which is stable below 598 °C. The composition ranges from 34 to 47 at% Pd at 400 °C
(2) a $PdCu_3$ phase with the $L1_2$ ($AuCu_3$) fcc-type structure which is stable below 508 °C for alloys with Pd less than ∼20 at%. Compositions with 20 to 27 at% Pd at 400 °C have a distorted $L1_2$ structure with a face-centered tetragonal atomic arrangement,[32] while compositions with 27 to 29 at% Pd at 400 °C have another distorted $L1_2$ structure with orthorhombic symmetry below 490 °C[33]
(3) an fcc-type solid solution phase with Cu randomly replaced by Pd can be found when the temperature and composition are outside of the two ranges mentioned above.

To compare the stability of different configurations, we used DFT calculations to optimize the structures described above. It is difficult to study the solid solution fcc structure because of the numerous possible structural configurations. Instead, we consider the two most common fcc-type binary alloys, $L1_1$ (the CuPt-type) and $L1_0$ (the AuCu-type). The $L1_1$-type alloy is layered along the [111] direction of the fcc cell, while the $L1_0$-type is layered along the [001] direction. $L1_1$ can be further deformed along the [111] direction and transformed to a B13 structure. These two structures are especially important for PdCu alloys as ORR catalysts, because the active surfaces are simultaneously close-packing and most stable.

The random solid solution phase is of less importance, because it has a short-range order or even a completely nonperiodic structure. Besides, there is little experimental evidence suggesting its existence for acid-treated catalysts.[13]

For the $PdCu_3$ composition, we consider the $L1_2$ ordered phase in which Cu is at the faces and Pd is at the corners of a cubic cell. We will not examine the distorted $L1_2$ structures, because they do not principally differ from the $L1_2$ structure. We also consider the random alloy. The $L1_2$ fcc-type structure is the only one that keeps all Pd atoms separated from each other. Hence, we consider an alternative structure with Pd appearing in pairs. The $L1_2$ structure is more stable (by 0.20 eV per $PdCu_3$ unit) than the random structure. This agrees with the fact that at low temperature $L1_2$ is a stable phase, while at higher temperature the alloy becomes a solid solution.

The 1:1 PdCu composition is of particular interest. The experimentally reported structure for this composition at temperatures lower than 598 °C is the B2 (or CsCl) structure, in which the cubic unit cell has Pd at the corners and Cu at the center. Thus, each atom has 8 neighbors instead of 12. At temperatures higher than 600 °C, Cu and Pd form a continuous fcc solid solution phase varying from pure Cu to pure Pd. It is difficult to generalize the catalytic activity for a solid solution because of the numerous possible structures. Taking into account that the $PdCu_3$ alloy has the ordered fcc structure, we assume that PdCu may also have a stable ordered phase related to fcc. Consequently, instead of a random PdCu structure, we optimized two fcc-like ordered phases for the PdCu composition. We considered the $L1_0$ structure (Figure 2) in which the Cu and

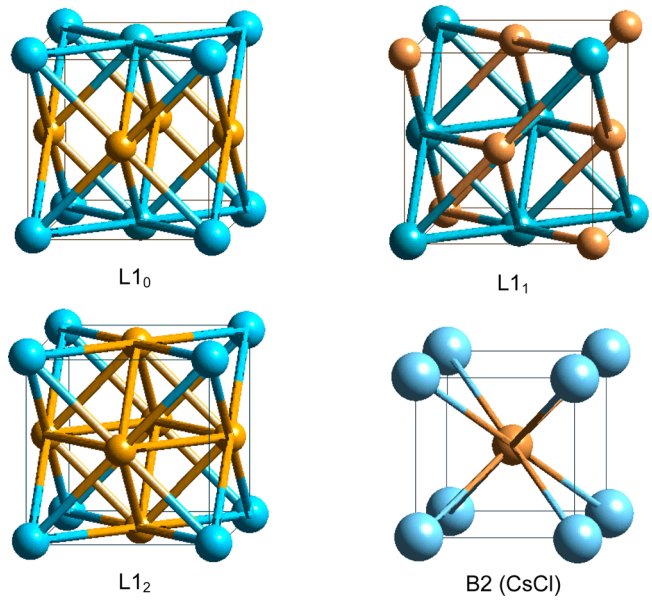

Figure 2. Possible structures for the PdCu systems.

Pd atoms are ordered along the [100] direction of the fcc unit cell and the $L1_1$ structure in which the Cu and Pd atoms are ordered along the fcc [111] direction. $L1_1$ can be deformed along the [111] direction and becomes a B13 structure, which is observed experimentally.[34] As shown in Table 1, we find the $L1_1$ and $L1_0$ phases are less stable (by 0.26 eV per PdCu unit) than the B2 structure.

We consider that the $L1_1$/B13 phase of PdCu could be a potentially interesting catalyst, because it has a layered structure in the close-packing direction. The $L1_0$ structure is also layered,

dx.doi.org/10.1021/cs4009623 | ACS Catal. 2014, 4, 1189−1197

Table 1. Calculated DFT Lattice Parameters (Å) Compared to Experimental Data (Values in Parentheses) and Corresponding Cohesive Energies (eV)

material	lattice parameter	cohesive energy per atom, QM
Pt	3.980 (3.97[36])	5.58
Cu (fcc)	3.66 (3.615[35])	3.63
Pd (fcc)	3.954 (3.90[36])	4.27
$PdCu_3$ ($L1_2$, fcc)	3.734 (3.676[34])	3.96
$PdCu_3$ (fcc solid solution)	N/A[a] (3.76[37])	3.91
PdCu (B_2, bcc)	3.020 (2.98[38])	4.17
PdCu ($L1_0$, fcc)	3.820[b] (N/A)	4.04
PdCu ($L1_1$/B13, fcc)	2.706[c] (2.700[38])	4.04
PdCu (fcc solid solution)	N/A[a] (3.765[38])	

[a]Lattice constant for the solid solution is unavailable as it allows numerous possible structures. [b]For the $L1_0$ structure, we use the fcc-type unit cell instead of the tetragonal for easier comparison. [c]For the $L1_1$ structure.

but its close-packing surface would always have half Cu and half Pd and hence is subject to much faster corrosion in the PEMFC acid environment. The $L1_1$ structure is layered in the close-packing direction. Thus, we can expect that the Cu plane could be oxidized off the surface, leaving the close-packing Pd surface exposed to the reactants at the PEMFC cathode.

Table 1 shows the DFT-predicted lattice parameters of Pd, Cu, Pt, and PdCu binary alloys compared to the experimental values and corresponding cohesive energies. For the pure Cu, Pd, and Pt phases, the lattice parameters are in general systematically larger (1.23%, 1,37%, and 1.45%, respectively) than the experimental values. For the PdCu binary alloys, lattice parameters of PdCu (B2), $PdCu_3$($L1_2$), and PdCu ($L1_0$ and $L1_1$) are 1.40%, 1.21%, and 1.58% larger, respectively, than the experimental values. Therefore, all above DFT-calculated lattice parameters are in good agreement with experiment.

In the next section, we will use the computationally optimized structures to examine the ORR.

3.2. Surface Structures and Energetics. It is well-known that the (111) surface is preferable for the fcc structure. For the $PdCu_3$-$L1_2$ structure, it is a close-packing (111) surface with 25% of the surface atoms being Pd. For the PdCu $L1_0$-structure, it is a close-packing (111) surface where one surface Pd connects to two subsurface Cu and one subsurface Pd (Figure 3). For PdCu-$L1_1$/B13, there are two unique close-packing surfaces, one with the surface Pd connecting to two sublayer Pd atoms and one Cu atom, and the other with the surface Pd connecting to a pure Cu subsurface. This surface is of particular interest, because it is less vulnerable to loss of Cu as compared to the case of the solid solution, $L1_0$ and nonlayered $L1_1$, where Cu can easily be leached out of the surface. It should be noted that due to technical issues, we do not compare here the relative stability of the facets considered for the $L1_1$ and $L1_0$ phases. In particular, for the layered PdCu-$L1_1$ surface structure, one side of the slab should be pure Pd and the other pure Cu to keep the 1:1 ratio. This would generate a net dipole along the *c* direction as result of the opposing charges of Cu and Pd (Cu has a positive charge, whereas Pd has a negative charge). The dipole would impose unrealistic interactions between the slabs arising due to the periodic boundary conditions, in particular along the *c* axis. There is no such problem for the nonlayered PdCu-$L1_1$ surface structure. Thus, the direct comparison of these two cases would be inappropriate, and therefore, we consider both cases in this paper.

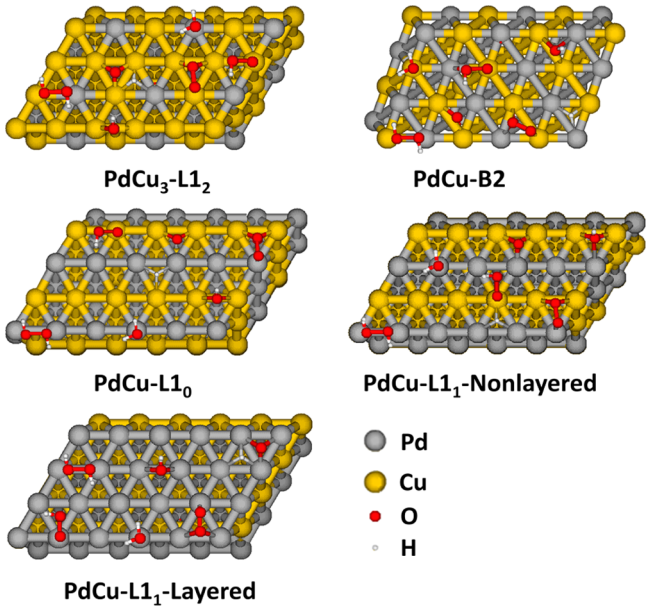

Figure 3. Top view of five alloy surfaces and the preferred binding sites for the ORR intermediates: H, O, OH, OOH, H_2O, O_2, and H_2O_2.

To avoid this dipole problem for the layered PdCu-$L1_1$ surface structure, we applied the five-layer PdCuPdCuPd slab for our further ORR adsorption and barrier calculations, where only relative energies are considered.

For the B2-type structure, it is not clear which surface is preferred. Hence, we carried out a surface cleavage study of all possible low index surfaces and calculated the corresponding surface energies. The six most stable surfaces are shown in Table 2.

Table 2. Six Most Stable Surfaces of the B2-Type PdCu Alloy

surface (*hkl*)	energy (eV/A^2)	energy (erg/cm^2)
PdCu(320)	0.135	2.16×10^3
PdCu(110)	0.136	2.17×10^3
PdCu(100)	0.145	2.32×10^3
PdCu(210)	0.147	2.36×10^3
PdCu(310)	0.151	2.41×10^3
PdCu(332)	0.152	2.43×10^3

The most preferable surfaces are (320) and (110). Including higher index surfaces leads to a group of surfaces with stability and structures similar to those of (320) and (110). All such high index surfaces can be viewed as (110) tilted with even smaller angles. Among all low index surfaces, (320) and (110) are most similar to the close-packing surface. This leads to the smallest surface area per atom and hence the highest stability. The (320) surface can be considered as the tilted (110) surface, or in other words, the (110) surface with steps as shown in Figure 4. Thus, we will focus on the (110) surface of the B2-type PdCu alloy.

A top view of five above-mentioned surfaces is shown in Figure 3.

3.3. ORR on Cu, Pt, PdCu, and $PdCu_3$. *3.3.1. Binding of ORR Intermediates.* We have studied the preferred binding sites of the ORR intermediates, such as O_{ad}, H_{ad}, O_{2ad}, OH_{ad}, H_2O_{ad}, OOH_{ad}, H_2O_{2ad}, on all surfaces of interest. Tables 3 and 4 show the binding energies of the ORR intermediates on the PdCu alloy surfaces in gas phase and solution. We also included the corresponding numbers for pure Pt, Pd, and Cu for comparison. All adsorbates prefer one of the four binding sites available on the (111) surface (Figure 5). These sites are denoted as μ_1 (top),

dx.doi.org/10.1021/cs4009623 | ACS Catal. 2014, 4, 1189−1197

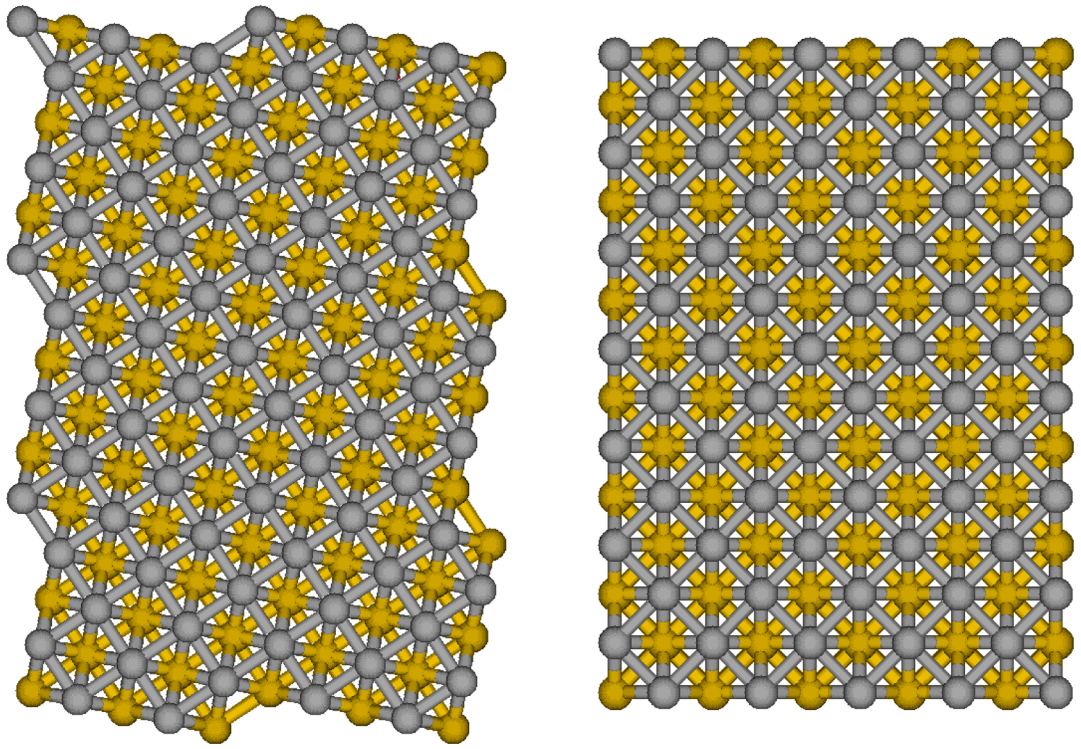

Figure 4. Side view of two most stable surfaces, PdCu-B2 (320) (left) and (110) (right).

Table 3. Binding Energies (eV) for the Intermediates Involved in ORR on Pt, Pd, Cu, and PdCu Alloys in Gas Phase

reaction intermediate	binding site	Pt	Pd	Cu	$PdCu_3$-$L1_2$[e]	PdCu-B2[e]	PdCu-$L1_0$[e]	PdCu-$L1_1$-nonlayered[e]	PdCu-$L1_1$-layered
H	μ_1	−2.90	−2.37	−2.03	−2.03	−2.24	−2.63	−2.81	−2.06
	μ_2[a]	−2.76	−2.68	−2.40	−2.49	−2.79	−2.61	−2.72	−2.52
	μ_3-fcc	−2.76	−2.79	−2.50	−2.60	−2.82[c]	−2.65	−2.79	−2.65
	μ_3-hcp	−2.75	−2.77	−2.51	−2.58	N/A[c]	−2.63	−2.58	−2.68
O	μ_1	−2.70	−2.52	−2.79	−2.54	−2.46	−2.27	−2.40	−2.05
	μ_2[b]	−3.33	−3.39	−4.05	−3.99	−3.93	−3.79	−3.76	−2.90
	μ_3-fcc	−3.90	−3.83	−4.40	−4.43	−3.93[c]	−3.75	−3.96	−3.35
	μ_3-hcp	−3.38	−3.63	−4.29	−3.98	N/A[c]	−3.94	−3.82	−3.19
OH	μ_1	−2.39	−2.32	−2.64	−2.42	−2.52	−2.22	−2.27	−1.95
	μ_2	−2.44	−2.54	−3.05	−2.68	−2.76	−2.53	−2.70	−2.16
	μ_3-fcc	−2.40	−2.50	−3.07	−2.69	−2.72[c]	−2.41	−2.67	−2.12
	μ_3-hcp	−2.50	−2.52	−3.05	−2.68	N/A[c]	−2.81	−2.55	−2.12
O_2	μ_2	−0.62	−0.74	−0.57	−0.45	−0.63	−0.45	−0.71	−0.36
	μ_3-fcc	−0.75	−0.81	−0.72	−0.61	−0.71[c]	−0.36	−0.62	−0.25
	μ_3-hcp	−0.58	−0.76	−0.71	−0.47	N/A[c]	−0.31	−0.54	−0.26
OOH	μ_{1b}	−1.20	−1.10	−1.27	−1.03	−1.18	−0.95	−0.94	−0.76
	μ_{1f}	−1.07	−1.05	−1.20	−0.90	N/A[d]	−0.91	−0.95	−0.77
H_2O_2	μ_2	−0.30	−0.36	−0.22	−0.24	−0.30	−0.26	−0.30	−0.28
H_2O	μ_1	−0.29	−0.26	−0.19	−0.24	−0.16	−0.24	−0.22	−0.25

[a]H is unstable at the μ_2 bridge site on Cu; the energy is for the saddle point between two 3-fold sites. [b]O is unstable at the μ_2 bridge site, which serves as a transition state for the surface diffusion. [c]For the PdCu-B2 surface, there are actually no such sites as fcc or hcp, because none of the sites has any atom beneath it. On the other hand, these two sites differ from each other, because one of them has two Pd adjacent atoms, while the other has two Cu adjacent atoms. For simplicity, we denote both sites as fcc and only show the better one. [d]The μ_{1f} site for OOH (one O atom is at the on-top position, while the second one is shifted toward the fcc position) is unstable for the PdCu-B2 alloy surface. The corresponding intermediate occupies the μ_{1b} site with the second O atom shifted toward the bridge position. [e]For these four structures, there are more sites than listed in the table due to the subsurface atom distribution. We calculated all possible sites, but since this table focuses on comparison between different alloys, for simplicity we only included the preferred sites of each type.

μ_2 (bridge), μ_3-fcc (fcc hollow), and μ_3-hcp (hcp hollow), according to the number of surface atoms to which the adsorbate binds.

In gas phase, H_{ad} prefers to bind to the μ_3-fcc sites on Pd, $PdCu_3$, B2-type PdCu, PdCu-$L1_0$, and nonlayered PdCu-$L1_1$ alloy surfaces, whereas for Cu and layered PdCu-$L1_1$, the μ_3-hcp site is slightly better. For pure Pt, the μ_1-top site is preferable for the H_{ad} binding.

Solvation greatly stabilizes the μ_1-top site, which becomes the most favorable site for $L1_0$ and nonlayered PdCu-$L1_1$, in addition

dx.doi.org/10.1021/cs4009623 | ACS Catal. 2014, 4, 1189−1197

Table 4. Binding Energies (eV) for Intermediates Involved in ORR on Pt, Pd, Cu, and PdCu Alloys in Solution

reaction intermediate	binding site	Pt	Pd	Cu	$PdCu_3$-$L1_2$[e]	PdCu-B2[e]	PdCu-$L1_0$[e]	PdCu-$L1_1$-nonlayered[e]	PdCu-$L1_1$-layered
H	μ_1	−2.97	−2.47	−2.05	−2.25	−2.71	−2.90	−3.22	−2.22
	μ_2[a]	−2.88	−2.82	−2.43	−2.61	−3.23	−2.87	−2.92	−2.67
	μ_3-fcc	−2.88	−2.94	−2.54	−2.67	−2.85[c]	−2.74	−2.88	−2.77
	μ_3-hcp	−2.87	−2.90	−2.54	−2.64	N/A[c]	−2.77	−2.85	−2.87
O	μ_1	−3.28	−3.13	−3.35	−3.04	−2.46	−2.90	−2.96	−2.77
	μ_2[b]	−3.96	−3.88	−4.51	−4.92	−4.40	−4.60	−4.18	−3.56
	μ_3-fcc	−4.60	−4.36	−4.90	−5.58	−4.37[c]	−4.77	−5.10	−4.03
	μ_3-hcp	−4.02	−4.15	−4.78	−4.90	N/A[c]	−4.55	−4.31	−3.89
OH	μ_1	−2.92	−2.79	−3.08	−2.87	−2.37	−2.69	−2.80	−2.58
	μ_2	−2.83	−2.90	−3.36	−3.04	−2.69	−2.95	−3.18	−2.69
	μ_3-fcc	−2.75	−2.81	−3.33	−3.02	−2.68[c]	−2.92	−3.19	−2.55
	μ_3-hcp	−2.86	−2.82	−3.31	−3.16	N/A[c]	−2.91	−2.87	−2.57
O_2	μ_2	−0.95	−0.89	−0.83	−0.70	−0.39	−0.73	−0.92	−0.61
	μ_3-fcc	−1.16	−1.05	−1.10	−1.16	−0.70[c]	−0.65	−0.88	−0.52
	μ_3-hcp	−0.93	−0.97	−1.09	−0.99	N/A[c]	−0.80	−0.81	−0.57
OOH	μ_{1b}	−1.66	−1.50	−1.73	−1.44	−1.13	−1.36	−1.36	−1.31
	μ_{1f}	−1.54	−1.48	−1.68	−1.38	N/A[d]	−1.29	−1.38	−1.35
H_2O_2	μ_2	−0.64	−0.66	−0.51	−0.58	−0.17	−0.53	−0.61	−0.67
H_2O	μ_1	−0.67	−0.60	−0.52	−0.61	−0.14	−0.56	−0.58	−0.70

[a]H is unstable at the μ_2 bridge site on Cu; the energy is for the saddle point between two 3-fold sites. [b]O is unstable at the μ_2 bridge site, which serves as a transition state for the surface diffusion. [c]For the PdCu-B2 surface, there are actually no such sites as fcc or hcp, because none of the sites has any atom beneath it. On the other hand, these two sites differ from each other, because one of them has two Pd adjacent atoms, while the other has two Cu adjacent atoms. For simplicity, we denote both sites as fcc and only show the better one. [d]The μ_{1f} site for OOH (one O atom is at the on-top position, while the second one is shifted toward the fcc position) is unstable for the PdCu-B2 alloy surface. The corresponding intermediate occupies the μ_{1b} site with the second O atom shifted toward the bridge position. [e]For these four structures, there are more sites than listed in the table due to the subsurface atom distribution. We calculated all possible sites, but since this table focuses on comparison between different alloys, for simplicity we only included the preferred sites of each type.

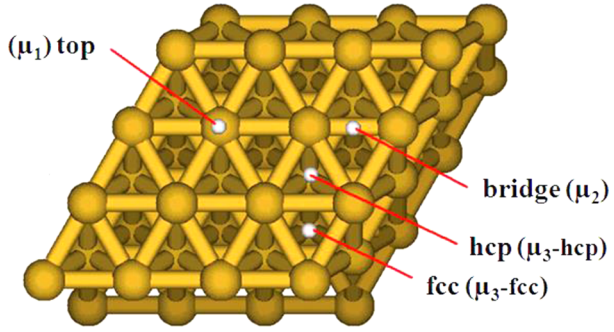

Figure 5. Four binding sites available on the (111) surface.

to pure Pt. The μ_2-bridge and μ_3-hcp sites are preferable for PdCu-B2 and layered PdCu-$L1_1$, respectively.

O_{ad} prefers binding to the μ_3-fcc site for Pd, Cu, Pt, and for all alloys, except for PdCu-B2 and PdCu-$L1_0$. For the B_2-type PdCu, the smaller distance between surface atoms, 2.62 Å as compared to 2.70 Å in pure Cu, helps improve the stability of the μ_2 site. For L_1- type PdCu, the preferred site is μ_3-hcp in gas phase and μ_3-fcc in solvent. For all mixed-metal surfaces (B2, $L1_0$, and nonlayered $L1_1$), sites with more adjacent Cu atoms are always more preferable, mostly due to stronger O_{ad} binding to Cu.

OH_{ad} prefers to bind to the μ_2, μ_3-fcc and μ_3-hcp sites with similar binding energies. This leads to a flat surface energy on the metals and high mobility of OH_{ad} given that the OH_{ad} can migrate through the μ_2 site. Similar to the case of O_{ad}, OH_{ad} prefers to bind to Cu on the surface than to Pd. Hence, for the striped $L1_0$ and $L1_1$ nonlayered structures, the migration is limited to the Cu line.

In gas phase, O_{2ad} prefers to bind to the μ_3-fcc site for Pt, Pd, Cu, $PdCu_3$, and PdCu-B2, while for PdCu-$L1_0$ and PdCu-$L1_1$, the μ_2-bridge site is preferable.

In solvent, the strongest binding energy of O_{2ad} corresponds to the μ_3-hcp site for PdCu-$L1_0$ and to the μ_2-bridge site for nonlayered PdCu-$L1_1$ and layered PdCu-$L1_1$. For Pt, Pd, Cu, $PdCu_3$, and PdCu-B2, O_{2ad} prefers the μ_3-fcc site. Again, the strong bond energy between O_{2ad} and Cu makes all sites connected with more Cu atoms preferable.

OOH_{ad} and H_2O_{ad} can only bind to the μ_1-top site for all materials studied. In all phases, except for PdCu-$L1_1$, OOH_{ad} prefers to have the O−O bond along a surface metal−metal bond.

Table 5. Barriers for the Reaction Steps Involved in ORR in Gas Phase

reaction barrier	Pt	Pd	Cu	$PdCu_3$-$L1_2$	PdCu-B2	PdCu-$L1_0$	PdCu-$L1_1$-nonlayered	PdCu-$L1_1$-layered
H_2 dissociation	0.00	0.00	0.16	0.66	0.19	0.29	0.24	0.42
O_2 dissociation	0.51	0.72	0.12	0.17	0.42	0.32	0.39	0.88
OH formation	0.82	0.27	0.00	0.37	0.46	0.01	0.07	0.00
OOH formation	0.34	0.50	0.37	0.37	0.76	0.26	0.30	0.39
OOH dissociation	0.01	0.32	0.49	0.32	0.05	0.17	0.24	0.65
O hydration	0.24	0.36	0.37	0.60	0.01	0.58	0.56	0.52
H_2O formation	0.12	0.53	0.84	0.86	0.82	0.60	0.56	0.41

dx.doi.org/10.1021/cs4009623 | ACS Catal. 2014, 4, 1189−1197

Table 6. Barriers for the Reaction Steps Involved in ORR in Solvated Phase

reaction barrier	Pt	Pd	Cu	$PdCu_3$-$L1_2$	PdCu-B2	PdCu-$L1_0$	PdCu-$L1_1$-nonlayered	PdCu-$L1_1$-layered
H_2 dissociation	0.00	0.00	0.04	0.56	0.00	0.22	0.06	0.19
O_2 dissociation	0.00	0.31	0.00	0.00	0.00	0.14	0.08	0.26
OH formation	1.23	0.42	0.14	0.81	0.96	0.07	0.17	0.38
OOH formation	0.25	0.65	0.43	0.44	1.10	0.40	0.41	0.54
OOH dissociation	0.00	0.04	0.31	0.13	0.00	0.00	0.06	0.17
O hydration	0.89	0.86	0.83	1.15	0.42	1.26	1.23	1.00
H_2O formation	0.24	0.76	0.94	0.86	0.99	0.60	0.59	0.45

Table 7. RDS Barriers for Four Possible ORR Mechanisms in Gas Phase[a]

reaction barrier	Pt	Pd	Cu	$PdCu_3$-$L1_2$	PdCu-B2	PdCu-$L1_0$	PdCu-$L1_1$-nonlayered	PdCu-$L1_1$-layered
O_2 dissociation	0.82^{1c}	0.72^{1b}	0.84^{1d}	0.86^{1d}	0.82^{1d}	0.60^{1d}	0.56^{1d}	0.88^{1b}
OOH formation	0.82^{2d}	0.53^{2e}	0.84^{2e}	0.86^{2e}	0.82^{2e}	0.60^{2e}	0.56^{2e}	0.65^{2c}
O_2 dissociation-hydration	0.51^{3b}	0.72^{3b}	0.84^{3d}	0.86^{3d}	0.82^{3d}	0.60^{3d}	0.56^{3d}	0.88^{3b}
OOH formation-hydration	0.34^{4b}	0.53^{4e}	0.84^{4e}	0.86^{4e}	0.82^{4e}	0.60^{4e}	0.56^{4e}	0.65^{4c}
overall	0.34	0.53	0.84	0.86	0.82	0.60	0.56	0.65

[a]Superscripts indicate reaction steps corresponding to the barriers.

3.3.2. Barriers for the Essential ORR Steps. In this section, we will discuss seven important steps involved in ORR:[14−18,38] (1) H_2 dissociation, (2) O_2 dissociation, (3) OH formation, (4) OOH formation, (5) OOH dissociation, (6) O hydration, and (7) H_2O formation. Tables 5 and 6 show corresponding barriers for these steps in gas phase and solution, respectively.

H_2 dissociation is easy on most surfaces with a barrier of 0.00−0.29 eV, except for $PdCu_3$ and layered PdCu-$L1_1$ with a barrier of 0.66 and 0.42 eV, respectively, in gas phase. The higher H_2 dissociation barriers are mostly due to the lower H_{ad} binding energy. This is worth noting as it shows how alloying with Cu dramatically changes the ORR activity, especially for the layered PdCu-$L1_1$ phase which has a pure Pd surface. Solvation generally makes the H_2 dissociation easier for all surfaces examined in this study.

O_{2ad} dissociation is easy on the $PdCu_3$ surface with a low barrier of 0.17 eV in gas phase, mostly due to stable O_{ad}. On PdCu surfaces of the B2 and $L1_0$ types, the reaction has a higher barrier of 0.42 and 0.32 eV, respectively. Layered PdCu-$L1_1$ has a high barrier of 0.88 eV due to the weak binding of O_{ad} (3.35 eV as compared to over 3.83 eV for the other alloys). Water solvation significantly decreases the barrier for both metals and metal alloys leading to the barrierless O_{2ad} dissociation for Pt, Cu, $PdCu_3$, PdCu-B2, and a low barrier of 0.14 eV for PdCu-$L1_0$ and 0.08 eV for nonlayered PdCu-$L1_1$. Pd and layered PdCu-$L1_1$ also have a much lower barrier of 0.31 and 0.26 eV, respectively.

OH_{ad} formation from O_{ad} + H_{ad} is easier on Cu, PdCu-$L1_0$, nonlayered PdCu-$L1_1$, and layered PdCu-$L1_1$ alloy surfaces as compared to the pure Pd surface. In gas phase, the barrier is 0.01 and 0.07 eV for PdCu-$L1_0$ and nonlayered PdCu-$L1_1$, respectively, which is lower comparing to 0.27 eV for Pd. For Cu and layered PdCu-$L1_1$, the reaction is barrierless in gas phase. In solution, the barrier becomes 0.14, 0.07, 0.17, 0.38, and 0.42 eV for Cu, PdCu-$L1_0$, nonlayered PdCu-$L1_1$, layered PdCu-$L1_1$ surfaces, and pure Pd, respectively. The OH_{ad} formation is harder on the Pt, B2, and $L1_2$-type PdCu surfaces with a barrier of 0.83, 0.46, and 0.37 eV in gas phase and 1.23, 0.96, and 0.81 eV in solution.

H_2O_{ad} formation from OH_{ad} + H_{ad} is very difficult on the Cu, PdCu-$L1_2$ and PdCu-B2 alloy surfaces with a barrier of 0.84, 0.86, and 0.82 eV in gas phase. PdCu-$L1_0$, nonlayered PdCu-$L1_1$, and pure Pd have lower barriers of 0.60, 0.56, and 0.53 eV, respectively. The reaction is easier on the layered PdCu-$L1_1$ surface with a barrier of 0.41 eV, which is significantly higher than that on Pt (0.12 eV). In solution, the barrier increases as solvation stabilizes OH_{ad} (see Table 6).

OOH_{ad} can be formed on the Pt, Cu, $PdCu_3$- $L1_2$, PdCu-$L1_0$, nonlayered PdCu-$L1_1$, and layered PdCu-$L1_1$ with barrier ranges from 0.26 to 0.39 eV in gas phase and 0.25−0.54 eV in solution (Tables 5 and 6). The reaction is more difficult for Pd and PdCu-B2 with a barrier of 0.50 and 0.76 eV in gas phase and 0.65 and 1.10 eV in solution, respectively.

The barrier for OOH_{ad} dissociation lies in the range of 0.01−0.65 eV in gas phase and 0.00−0.31 eV in solution. The highest barrier, 0.65 eV, in gas phase is for the layered PdCu-$L1_1$ structured surface and the lowest, 0.01 eV, is for Pt. In solution, the highest barrier is 0.31 eV for the OOH dissociation on the Cu surface, while it is barrierless for pure Pt.

For metals with high OH_{ad} formation barriers, O_{ad} can react with a surface H_2O_{ad} to form two OH_{ad} directly. This is especially important for surfaces like Pt(111), where the direct OH_{ad} formation is relatively difficult. The barrier ranges from 0.01 to 0.58 eV in gas phase. Solvation makes the reaction extremely difficult, because the barrier becomes higher than 0.83 eV for all surfaces except for PdCu-B2, where the barrier is 0.42 eV.

3.3.3. Possible ORR Mechanisms and Rate-Determining Steps. Analyzing the ORR steps, we can find the rate-determining step (RDS) for possible ORR mechanisms. Here, we assume that the reaction step with the highest barrier is the RDS. It should be noted that to really determine the RDS, a thermodynamic and kinetic analysis needs to be performed, but this would require additional information about the adsorbate surface concentration and distribution and some other special factors, which can hardly be found in the literature. We do not consider the influence of the electrode potential on the ORR steps either. The problem of calculating barriers for a redox reaction in electrochemical systems is that the actual electron transfer process is not explicitly included in the barrier. Some researchers (see, for instance, refs 39 and 40) made several key physical assumptions to justify that their DFT calculated barriers can be used to estimate the redox barrier. To avoid such disputable physical assumptions, we estimated the general energetics of the ORR at zero external potential. Such a

dx.doi.org/10.1021/cs4009623 | ACS Catal. 2014, 4, 1189−1197

Table 8. RDS Barriers for Four Possible ORR Mechanisms in Solvated Phase[a]

reaction barrier	Pt	Pd	Cu	$PdCu_3$-$L1_2$	PdCu-B2	PdCu-$L1_0$	PdCu-$L1_1$-nonlayered	PdCu-$L1_1$-layered
O_2 dissociation	1.23^{1c}	0.76^{1d}	0.94^{1d}	0.86^{1d}	0.99^{1d}	0.60^{1d}	0.59^{1d}	0.45^{1d}
OOH formation	1.23^{2d}	0.76^{2e}	0.94^{2e}	0.86^{2e}	1.10^{2b}	0.60^{2e}	0.59^{2e}	0.54^{2b}
O_2 dissociation-hydration	0.89^{3c}	0.86^{3c}	0.94^{3d}	1.15^{3c}	0.99^{3d}	1.26^{3c}	1.23^{3c}	1.00^{3c}
OOH formation-hydration	0.89^{4d}	0.86^{4d}	0.94^{4e}	1.15^{4d}	1.10^{4b}	1.26^{4d}	1.23^{4d}	1.00^{4d}
Overall	0.89	0.76	0.94	0.86	0.99	0.60	0.59	0.45

[a]Superscripts indicate reaction steps corresponding to the barriers.

simplified approach provides a consistent way to estimate the energetics of this reaction.

As discussed in our earlier published paper,[16] there are four feasible mechanisms for ORR on Pt surface: (1) O_2 dissociation, (2) OOH formation, 3) O_2 dissociation-hydration, and (4) OOH formation-hydration. Tables 7 and 8 include the corresponding RDS barriers in gas phase and solvent, respectively.

O_2-Dissociation Mechanism. In this mechanism, O_{2ad} dissociates into two O_{ad}, which further react with $2H_{ad}$ to form, first, OH_{ad}, and then H_2O_{ad}. The steps involved in this mechanism are

$$O_{2g} \rightarrow O_{2ad} \quad (1a)$$

$$O_{2ad} \rightarrow 2O_{ad} \quad (1b)$$

$$O_{ad} + H_{ad} \rightarrow OH_{ad} \quad (1c)$$

$$OH_{ad} + H_{ad} \rightarrow H_2O_{ad} \quad (1d)$$

The RDS barrier for this mechanism varies from 0.56 eV for nonlayered PdCu-$L1_1$ to 0.88 eV for layered PdCu-$L1_1$ in gas phase (Table 7). For most surfaces, such as Pd, Cu, $PdCu_3$-$L1_2$, PdCu-B2, PdCu-$L1_0$, and nonlayered PdCu-$L1_1$, the RDS is the H_2O formation (step 1d), while for Pd and layered PdCu-$L1_1$, the RDS is the O_2 dissociation (step 1b). Only for Pt, the RDS is the OH formation reaction (step 1c) with a barrier of 0.82 eV.

In solvent, for almost all surfaces, the RDS is the H_2O formation reaction (step 1d) with a barrier ranging from 0.45 eV for layered PdCu-$L1_1$ to 0.99 eV for PdCu-B2 (Table 8). Only for Pt, the OH formation reaction (step 1c) with a barrier of 1.23 eV remains the RDS for the O_2-dissociation mechanism.

OOH-Formation Mechanism. When it is difficult for O_2 to directly dissociate on the surface (for example, Pd and layered PdCu-$L1_1$ in gas phase), this species could react, first, with H_{ad} to form OOH_{ad}, and then OOH_{ad} dissociates into O_{ad} and OH_{ad}. The reaction steps for this mechanism are as follows

$$O_{2g} \rightarrow O_{2ad} \quad (2a)$$

$$H_{ad} + O_{2ad} \rightarrow OOH_{ad} \quad (2b)$$

$$OOH_{ad} \rightarrow OH_{ad} + O_{ad} \quad (2c)$$

$$O_{ad} + H_{ad} \rightarrow OH_{ad} \quad (2d)$$

$$OH_{ad} + H_{ad} \rightarrow H_2O_{ad} \quad (2e)$$

In gas phase, the RDS for the OOH-formation mechanism varies from 0.53 eV for Pd to 0.86 eV for $PdCu_3$-$L1_2$ (Table 7). For most surfaces, the RDS is the H_2O formation step 2d, except for layered PdCu-$L1_1$ and pure Pt, where the RDS is the OOH dissociation (step 2c) with a barrier of 0.65 eV and OH formation (step 2d) with a barrier of 0.82 eV, respectively.

In solvated phase, the RDS for Pt remains the OH formation reaction with a barrier of 1.23 eV, the same as in the O_2-dissociation mechanism (Table 8). For PdCu-B2 and layered PdCu-$L1_1$, the OOH-formation step 2b is the RDS with a barrier of 1.10 and 0.54 eV, respectively. For all other surfaces, the RDS is the H_2O-formation reaction (step 2e) with a barrier ranging from 0.59 eV for nonlayered PdCu-$L1_1$ to 0.94 eV for Cu.

Overall, this mechanism still includes the OH formation and H_2O formation steps, similar to the O_2-dissociation mechanism.

O_2-Dissociation-Hydration Mechanism. As we proposed in our earlier publication,[16] an alternative mechanism might be considered for surfaces like Pt(111), where the direct OH formation step is energetically unfavorable. OH can be formed via a hydration step, in which O_{ad} reacts with a surface H_2O to form 2OH with a much lower barrier.

$$O_{2g} \rightarrow O_{2ad} \quad (3a)$$

$$O_{2ad} \rightarrow 2O_{ad} \quad (3b)$$

$$O_{ad} + H_2O_{ad} \rightarrow 2OH_{ad} \quad (3c)$$

$$OH_{ad} + H_{ad} \rightarrow H_2O_{ad} \quad (3d)$$

In this mechanism, the RDS in gas phase is the O_2 dissociation reaction (step 3b) for Pt, PdCu-B2, and layered PdCu-$L1_1$ surfaces with barriers of 0.51, 0.72, and 0.88 eV, respectively (Table 7). For all other surfaces, the RDS is the H_2O formation reaction (step) with a barrier that varies from 0.56 eV for nonlayered PdCu-$L1_1$ to 0.86 eV for $PdCu_3$-$L1_2$.

In water solvent, the RDS is the hydration reaction (step 3d) for most of the surfaces with a barrier ranging from 0.86 eV for Pd to 1.26 eV for PdCu-$L1_0$ (Table 8). Only Cu and PdCu-B2 have the H_2O formation reaction (step 3d) as the RDS with a barrier of 0.94 and 0.99 eV, respectively.

OOH-Formation-Hydration Mechanism. The OOH-formation mechanism can also involve the hydration reaction to form OH_{ad}. Here, the reaction steps are

$$O_{2g} \rightarrow O_{2ad} \quad (4a)$$

$$H_{ad} + O_{2ad} \rightarrow OOH_{ad} \quad (4b)$$

$$OOH_{ad} \rightarrow OH_{ad} + O_{ad} \quad (4c)$$

$$O_{ad} + H_2O_{ad} \rightarrow 2OH_{ad} \quad (4d)$$

$$OH_{ad} + H_{ad} \rightarrow H_2O_{ad} \quad (4e)$$

In gas phase, for the Pt and layered PdCu-$L1_1$ surfaces, the RDS is the OOH formation reaction (step 4b) and OOH dissociation reaction (step 4c) with barriers of 0.34 and 0.65 eV, respectively (Table 7). For all other surfaces, the RDS is the H_2O formation reaction (step 4e) with a barrier ranging from 0.53 eV for Pd to 0.86 eV for $PdCu_3$-$L1_2$.

In solution, the RDS is the hydration reaction (step 4d) for most of the surfaces with a barrier ranging from 0.86 eV for Pd to 1.26 eV for PdCu-$L1_0$ (Table 8). Only Cu and PdCu-B2 have the H_2O formation reaction (step 4e) and the OOH formation reaction (step 4b) as the RDS with a barrier of 0.94 and 1.10 eV, respectively.

dx.doi.org/10.1021/cs4009623 | ACS Catal. 2014, 4, 1189−1197

Summarizing this section, we can conclude that for Pd, Cu, and all PdCu alloys, the predicted ORR mechanism is O_2-dissociation with the H_2O formation reaction as the RDS. In gas phase, Pd and nonlayered PdCu-$L1_1$ have similar, relatively low RDS barriers of 0.53 and 0.56 eV, respectively. In water solvent, the layered PdCu-$L1_1$ alloy has the lowest RDS barrier of 0.45 eV, followed by the nonlayered PdCu-$L1_1$ and PdCu-$L1_0$ alloys with the similar RDS barriers of 0.59 and 0.60 eV. The small difference in the barriers can be explained by the structural similarity between these two surfaces, both of which have alternating Pd and Cu lines in each layer. We can expect that the above-mentioned PdCu alloys may have a better catalytic performance, while Cu, $PdCu_3$-$L1_2$, and PdCu-B2 with the RDS barriers of 0.94, 0.86, and 0.99 eV, respectively, will show a worse performance, than pure Pd with the RDS barrier of 0.76 eV. Overall, three PdCu alloys—layered PdCu-$L1_1$, nonlayered PdCu-$L1_1$, and PdCu-$L1_0$—show a significant improvement in the RDS barriers relative to pure Pd.

Comparing pure Pt and Pd, we would like to note that the 2×2 lattice surface structure used in this work predicts a better performance of Pt in gas phase but worse in water solvent. The latter contradicts the experimental results observed. However, using the 3×3 lattice surface structure dramatically decreases the O hydration barrier to 0.50 eV for Pt and 0.49 eV for Pd in solution. This is due to the fact that the O hydration step requires a lower coverage because of the longer reaction path. On the other hand, the H_2O formation reaction step generally does not depend on the choice of the lattice surface structure. The H_2O formation barrier using the 3×3 lattice surface structure is 0.24 eV for Pt and 0.78 eV for Pd, practically the same as those calculated using the 2×2 lattice surface structure. Thus, only Pt significantly (0.4 eV) benefits from the decrease of the barrier for the oxygen hydration step so that the O_2-dissociation-hydration mechanism becomes favorable for Pt.[16] The inclusion of the hydration step in the ORR mechanisms for Pd, Cu, and all PdCu alloys studied here does not improve the situation, because the RDS for these materials is the H_2O formation reaction, unlike Pt where the RDS is the OH formation.

3.4. Comparison to Experimental Results. Figure 6 shows the experimental mass activity of various PdCu colloidal catalysts[13] compared to Pt. As expected, the mass activity of Pt is much higher than Pd, ~1450 and 200 mA/mg, respectively. However, the mass activity of PdCu alloys is significantly higher than pure Pd, ~800 mA/mg for PdCu and ~600 mA/mg for $PdCu_3$. This result is consistent with our computational findings.

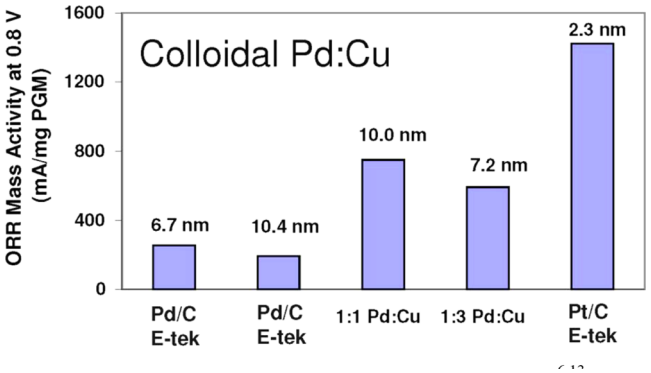

Figure 6. Mass activity of Pt, Pd, and PdCu alloy catalysts.[6,13] The 1:1 PdCu catalyst has performance about half as good as Pt and over twice as good as Pd.

From the X-ray diffraction patterns of the PdCu catalysts,[13] the structure was determined as disordered fcc rather than the bcc-like (B2), which was earlier observed experimentally to be the stable phase for this composition.[37] This is probably due to the heat treatment above the order/disorder phase transition temperature performed in the former case. Indeed, as we showed in sections 3.3.2 and 3.3.3, the bcc-type structure would have a poor performance, whereas the ordered $L1_1$ phase is predicted to have a much better performance. This suggests that the heat treatment might facilitate the formation of the phase favorable for ORR. The acid treatment probably helps this process by removing the disordered components.

4. CONCLUSIONS

Using DFT calculations, we have computationally studied PdCu alloy catalysts as possible non-Pt catalysts for ORR. The structural preference and ORR activity as a function of the composition and surface structure were determined. Five PdCu alloy surface structures (i.e., B2, $L1_2$, $L1_0$, $L1_1$-nonlayered, and $L1_1$-layered) were considered, and the layered $L1_1$ surface was found to exhibit a significant improvement of the ORR barriers in solvated phase, compared to those for pure Pd. The RDS for ORR on the layered PdCu-$L1_1$, nonlayered PdCu-$L1_1$, and PdCu-$L1_0$ surfaces in solution is the H_2O formation reaction with a barrier of 0.45, 0.59, and 0.60 eV, respectively. Our computational result is generally consistent with the experimental data.[13]

AUTHOR INFORMATION

Corresponding Authors

*E-mail: (B.V.M.) merinov@caltech.edu.
*E-mail: (W.A.G.) wag@wag.caltech.edu.

Notes

The authors declare no competing financial interest.

ACKNOWLEDGMENTS

We thank Drs. Deborah Myers, John Regalbuto, and Christian Heske for fruitful discussions. Financial support from the U.S. Department of Energy (contract no. DE-AC02-06CH11357) and from the National Science Foundation (grant CBET-1067848) is gratefully acknowledged. The facilities of the Materials and Process Simulation Center used in this study were established with grants from DURIP-ONR, DURIP-ARO, and NSF-CSEM.

REFERENCES

(1) Kordesch, K.; Simader, G. *Fuel Cell and their Applications*; VCH: New York, 1996.
(2) Appleby, A.; Foulkes, F. *Fuel Cell Handbook*; Van Nostrand Reinhold: New York, 1989.
(3) Brandon, N. P.; Skinner, S.; Steele, B. C. H. *Annual Rev. Mater. Res.* **2003**, *33*, 183−213.
(4) Mehta, V.; Cooper, J. S. *J. Power Sources* **2003**, *114*, 32−53.
(5) Ahluwalla, R. K.; Wang, X.; Lajunen, A.; Steinbaach, A. J.; Hendricks, S. M.; Kurkowski, M. J.; Debe, M. K. *J. Power Sources* **2012**, *215*, 77−88.
(6) Bard, A. J.; Parsons, R.; Jordan, J. *Standard Potentials in Aqueous Solutions*, International Union of Pure and Applied Chemists; , Marcel Dekker: New York, 1985.
(7) Kinoshita, K. *Electrochemical Oxygen Technology*; John Wiley & Sons: New York, 1992.
(8) Ruban, A.; Hammer, B.; Stoltze, P.; Skriver, H. L.; Nørskov, J. K. *J. Mol. Catal. A* **1997**, *115*, 421−429.
(9) Hammer, B.; Nørskov, J. K. *Surf. Sci.* **1995**, *343*, 211−220.

(10) Hammer, B.; Nørskov, J. K. *Adv. Catal.* **2000**, *45*, 71−129.
(11) Stamenkovic, V.; Mun, B. S.; Mayrhofer, K. J. J.; Ross, P. N.; Markovic, N. M.; Rossmeisl, J.; Greeley, J.; Nørskov, J. K. *Angew. Chem., Int. Ed.* **2006**, *45*, 2897−2901.
(12) Nørskov, J. K.; Rossmeisl, J.; Logadottir, A.; Lindqvist, L.; Kitchin, J. R.; Bligaard, T.; Jónsson, H. *J. Phys. Chem. B* **2004**, *108*, 17886−17892.
(13) Wang, X. P.; Kariuki, N.; Vaughey, J. T.; Goodpaster, J.; Kumar, R.; Myers, D. J. *J. Electrochem. Soc.* **2008**, *155*, B602−B609.
(14) Sha, Y.; Yu, T. H.; Liu, Y.; Merinov, B. V.; Goddard, W. A. *J. Phys. Chem. Lett.* **2010**, *1*, 856−861.
(15) Sha, Y.; Yu, T. H.; Merinov, B. V.; Shirvanian, P.; Goddard, W. A. *J. Phys. Chem. C* **2012**, *116*, 21334−21342.
(16) Sha, Y.; Yu, T. H.; Merinov, B. V.; Shirvanian, P.; Goddard, W. A. *J. Phys. Chem. Lett.* **2011**, *2*, 572−576.
(17) Yu, T. H.; Sha, Y.; Merinov, B. V.; Goddard, W. A. *J. Phys. Chem. C* **2010**, *144*, 11527−11533.
(18) Sha, Y.; Yu, T. H.; Merinov, B. V.; Goddard, W. A. *J. Phys. Chem. C* **2012**, *116*, 6166−6173.
(19) Schultz, P. *SeqQuest Code Project*; Sandia National Laboratories: Albuquerque, NM. http://www.cs.sandia.gov/~paschul/Quest/ (accessed Dec. 3, 2004)
(20) Melius, C. F.; Goddard, W. A. *Phys. Rev. A* **1974**, *10*, 15280−1540.
(21) Melius, C. F.; Olafson, B. D.; Goddard, W. A. *Chem. Phys. Lett.* **1974**, *28*, 457−462.
(22) Redondo, A.; Goddard, W. A.; Mcgill, T. C. *Phys. Rev. B* **1977**, *15*, 5038−5048.
(23) Hamann, D. R. *Phys. Rev. B* **1989**, *40*, 2980−2987.
(24) Perdew, J.; Burke, K.; Ernzerhof, M. *Phys. Rev. Lett.* **1996**, *77*, 3865−3868.
(25) Tomasi, J.; Persico, M. *Chem. Rev.* **1994**, *94*, 2027−2094.
(26) Cramer, C.; Truhlar, D. *Chem. Rev.* **1999**, *99*, 2161−2200.
(27) Tannor, D. J.; Marten, B.; Murphy, R.; Friesner, R. A.; Sitkoff, D.; Nicholls, A.; Ringnalda, M.; Goddard, W. A.; Honig, B. *J. Am. Chem. Soc.* **1994**, *116*, 11875−11882.
(28) Baker, N.; Sept, D.; Joseph, S.; Holst, M.; McCammon. *J. Proc. Natl. Acad. Sci. U.S.A.* **2001**, *98*, 10037−10041.
(29) Mills, G.; Jonsson, H.; Schenter, G. K. *Surf. Sci.* **1995**, *324*, 305−337.
(30) Mills, G.; Jonsson, H. *Phys. Rev. Lett.* **1994**, *72*, 1124−1127.
(31) Subramanian, P. R., Laughlin, D. E., In *Binary Alloy Phase Diagrams*, 2nd ed.; Massalski, T. B., Okamoto, H., Subramanian, P. R., Kacprzak, L.; Eds.; ASM International: Materials Park, OH, 1990; Vol. 2, p 1454.
(32) Ohshima, K.; Watanabe, D. *Acta Crystallogr., Sect. A: Cryst. Phys., Diffr., Theor. Gen. Crystallogr.* **1973**, *29*, 520−526.
(33) Watanabe, D.; Ogawa, S. *J. Phys. Soc. Jpn.* **1956**, *11*, 226−239.
(34) Guymont, M.; Gratias, D. *Phys. Status Solidi A* **1976**, *36*, 329−334.
(35) Otte, H. M. *J. Appl. Phys.* **1961**, *32*, 1536−1546.
(36) Haglund, J.; Guillermet, A. F.; Grimvall, G.; Korling, M. *Phys. Rev. B* **1993**, *48*, 11685−11691.
(37) Yusenko, K. V.; Filatov, E. Y.; Vasilchenko, D. B.; Baidina, I. A.; Zadesenez, A. V.; Shubin, Y. V. *Zeit. Kristallogr.* **2007**, *26*, 289−295.
(38) Jacob, T.; Goddard, W. A. *ChemPhysChem* **2006**, *7*, 992−1005.
(39) Filhol, J. S.; Neurock, M. *Angew. Chem., Int. Ed.* **2006**, *45*, 402−406.
(40) Janik, M. J.; Taylor, C. D.; Neurock, M. *J. Electrochem. Soc.* **2009**, *156*, B126−B135.